urban science

MDPI

Article

Islanding Detection in Grid-Connected Urban Community Multi-Microgrid Clusters Using Decision-Tree-Based Fuzzy Logic Controller for Improved Transient Response

Yellapragada Venkata Pavan Kumar [1,2,*], Sivakavi Naga Venkata Bramareswara Rao [3] and Ramani Kannan [2]

[1] School of Electronics Engineering, VIT-AP University, Amaravati 522237, Andhra Pradesh, India
[2] Department of Electrical and Electronics Engineering, Universiti Teknologi Petronas (UTP), Seri Iskandar 32610, Perak, Malaysia; ramani.kannan@utp.edu.my
[3] Department of Electrical and Electronics Engineering, Sir C. R. Reddy College of Engineering, Eluru 534007, Andhra Pradesh, India; snvbrao.eee@sircrrengg.ac.in
* Correspondence: pavankumar.yv@vitap.ac.in; Tel.: +91-863-2370155

Abstract: The development of renewable-energy-based microgrids is being considered as a potential solution to lessen the unrelenting burden on the centralized utility grid. Furthermore, recent studies reveal that integrated multi-microgrid cluster systems developed in urban communities maximize the effectiveness of microgrids and greatly decrease the utility grid dependence. However, due to the uncertain nature of renewable energy sources and frequent load variations, these systems face issues with unintentional islanding operations. This can create severe damage to the microgrid's performance in its stable operating condition and lead to undesired transient responses. Hence, islanding must be identified rapidly to take preventive measures to address the issue. This requires the development of a suitable anti-islanding technique that is faster in terms of accuracy and timely detection. With this intention, this paper proposes a decision-tree-based fuzzy logic (DT-FL) controller for the rapid identification of islands in an urban community multi-microgrid cluster. The DT-FL controller's operation includes two steps. First, the decision tree extracts the electrical parameters at the point of common coupling of the multi-microgrid system. Second, these extracted parameters are utilized for the online tuning of the fuzzy logic controller, for the fast detection of islanding. The multi-microgrid cluster under study, along with the proposed islanding technique, is implemented in the MATLAB-2021a software. The efficacy of the proposed DT-FL controller is validated by comparing its performance with that of the conventional fuzzy logic controller under different test scenarios. From the results, it is observed that the proposed DT-FL controller shows superior performance in terms of the islanding detection time as well as the transient response of the system when compared with the conventional controller.

Keywords: cluster microgrids; community microgrids; decision tree; fuzzy logic controller; islanding detection; microgrid; multi-microgrids; transient response; urban community

Citation: Venkata Pavan Kumar, Y.; Naga Venkata Bramareswara Rao, S.; Kannan, R. Islanding Detection in Grid-Connected Urban Community Multi-Microgrid Clusters Using Decision-Tree-Based Fuzzy Logic Controller for Improved Transient Response. *Urban Sci.* **2023**, *7*, 72. https://doi.org/10.3390/urbansci7030072

Academic Editor: Luis Hernández-Callejo

Received: 15 April 2023
Revised: 10 June 2023
Accepted: 29 June 2023
Published: 3 July 2023

1. Introduction

The demand for electrical energy is a useful tool for measurement in the economy of any country around the world. Energy demands have become more complex as a result of the rising standards of living worldwide. By 2050, the urban population is anticipated to rise from 55% to 69%, resulting in a massive energy demand [1,2]. Moreover, the energy sector's continuous urbanization and growth has significantly increased the load on the electric grid, leading to frequent grid failures. All of these elements have paved the way to the installation of distributed generation (DG) systems, which will lessen the reliance on the utility grid [3]. Hence, local energy-producing facilities based on renewable energy are added to the conventional central utility system [4,5]. Over the past several years, improvements in distributed generators (DGs) have been essential in addressing problems

with traditional power system networks. A probable solution to the unavailability and exhaustion of fossil fuels, as well as to the rapid increase in electric load, environmental pollution, and the high costs of petroleum products and gases, may be found in the significant rise of DGs. A range of technological, governmental, and current issues in the conventional electric system have been successfully addressed by DGs [6]. This groundbreaking technology has led to the replacement of the conventional electric power system with microgrids, which are low-voltage active distribution systems. A microgrid (MG) is a network of energy storage, distributed generation (DG), and various loads that can be managed by monitoring and protection systems. Circuit breakers are typically used at the point of common connection to link microgrids to the main grid on the distribution side (PCC). The MG is synchronized with the utility under normal operating conditions and will be disconnected from the utility grid and operate in an autonomous mode to meet high energy demands if it experiences any problems, such as voltage or frequency variations [7]. The DG units in a microgrid have substantially less capacity than the enormous generators used in traditional systems; the MG is vulnerable to climate change due to its lower energy density and dependency on regional topographical considerations. Because of their proximity to consumers, they can supply electricity and heat loads with the proper voltage and frequency while minimizing transmission losses, preventing the power network from becoming congested. By keeping the lights on when the regular power source is available, they raise the technical standards, economic benefits, and environmental reliability of the current power system. These interruptions might cause significant changes in some system characteristics, which might result in instability in the power system. Therefore, it is important to identify and fix any disturbances as soon as possible to maintain the continuity of the power supply. Several utilities view the islanded operation mode of DG units as a feasible strategy to preserve continuity and reliability due to the significant diffusion of renewable energy resources (RES) in distribution systems. However, islanding operations require a quick, accurate, and economical islanding detection method, which has no impact on the supply's quality. As a result, several islanding control mechanisms have been created and implemented on these DG units. According to IEEE Std. 1547-2003 [8], islanding must be identified within 2 s of it taking place. The following are the literature works that have discussed the islanding techniques that are used in a microgrid system.

The authors of [9] proposed a hybrid method for islanding detection to identify the islanding phenomenon in a distribution system. The proposed approach is a hybrid technique that combines a passive approach and a remote detection approach. The next stage is the proposal of an adaptive control method to guarantee the steady operation of islanded subsections. The proposed technique makes use of error rates for system parameters such as voltage and power to re-adjust generator controls and keep the system stable. In [10], the researchers suggest a unique islanding detection approach based on an adaptive neuro-fuzzy inference system (ANFIS) that is integrated with various passive monitoring strategies. One of the objectives of this study is to minimize the negative effects of the islanding detection (IDT) approach on PQ, while preserving the detection accuracy and minimizing the non-detection zone (NDZ). The suggested method's main component is data mining, which enables all necessary data to be obtained using relay metering sensors installed on the PCC. To create a decentralized IDT for numerous and hybrid DG-based microgrids, each DG connected at the PCC in [11] injects a low-frequency disturbance signal through a d-axis current controller that is integrated with the suggested hybrid analysis technique. The suggested approach is capable of identifying island formation due to (1) individual DGs becoming isolated from the rest of the system, with or without a load, and (2) additional DGs becoming isolated from the grid with or without a load. The study in [12] suggests a novel method for the quick identification of islanding events in a microgrid (MG). The suggested method consists of two steps, the first of which is to extract certain useful features from the voltage and current information. The discrete Fourier transform is used to examine these signals for the second harmonic termination (DFT). LSTM is a novel artificial intelligence method that uses a unique recurrent neural network structure. In [13],

a passive IDT based on the rate of change of frequency deviation technique is investigated within the MG under various levels of power imbalance. Moreover, [14] demonstrates the phenomenon as quickly and accurately as possible using the rate of change of power technique based on the terminal voltage of a photovoltaic inverter. However, in [15], the authors extracted electrical feature quantities that had a strong correlation with islanding detection. In addition, an islanding detection method based on CatBoost was proposed for an MG in this paper to effectively determine the thresholds of multiple electrical feature quantities and reduce the dead zone in the islanding detection process. The authors in [16] used the superimposed angle of negative sequence impedance for the detection of islands in a reconfigurable system. The authors in [17] used a combinatorial strategy combining various passive schemes in an attempt to reduce the detection time and the non-detection zone (NDZ). However, the authors in [18] proposed a hybrid active and passive islanding technique. The method was used to obtain a solution for the NDZ by using fuzzy classifiers and applying a suitable active or passive method. An approach to unplanned island detection in a microgrid with a micro-phasor measurement unit is suggested in [19]. To determine if an island or fault will develop, the unit extracts specific features from recorded voltage data utilizing the discrete fractional Fourier transform's multi-domain nature.

From the literature, it is identified that the development of knowledge-based classifiers frequently relies on classification methods based on decision tree, Bayes classification, and SVM approaches. Deep learning methodologies are now most frequently used when creating classification algorithms. When there are enormous amounts of data accessible, these strategies are highly useful. However, gathering such information for educational purposes might be challenging. Thus, one of the best ways to visualize a decision in these situations is through a decision tree. When the next step in the decision-making process depends on the information analysis from previous steps, a decision tree can be interpreted as a representation of regular human reasoning. Moreover, studies in the literature have focused on implementing classification methods to determine islanding in single microgrid systems. Thus, by keeping these aspects in view, this paper proposes a decision-tree-based fuzzy controller for effective islanding detection with an improved transient response in a multi-microgrid system, which is formed by integrating two adjacent microgrids in an urban community.

The remainder of the article is structured as follows. Section 2 presents the description of the system under study and also the modeling of the various constituent units of the system; Section 3 discusses the proposed decision-tree-based fuzzy logic controller; Section 4 presents a discussion of the simulation findings; and the conclusions are presented in Section 5.

2. Description and Modeling of Multi-Microgrid (MMG) System under Study

The architecture of a multi-microgrid system in an urban community, which is entirely based on the AC power park, is illustrated in Figure 1. The system consists of two microgrids, each of which is viewed as a standalone structure functioning in a remote location with a constant AC voltage of 415 V. Each MG is associated with different energy sources, DC/DC converters, and building loads. Because the voltage generated by renewable energy sources is low, it is boosted to a value of 500 V (DC), which is comparable to 415 V of AC voltage. The individual MGs are modeled to operate in both isolated and grid-connected modes. The multi-microgrid system under study is connected to a utility grid via the point of common coupling. MG-1 is modeled with a solar PV energy source with the MPPT algorithm, a DC/DC converter, a 3-Φ inverter, and residential building loads. Similarly, MG-2 is modeled with a fuel cell, DC/DC converter, 3-Φ inverter, and academic institute building loads. All component ratings are given in Appendix A.

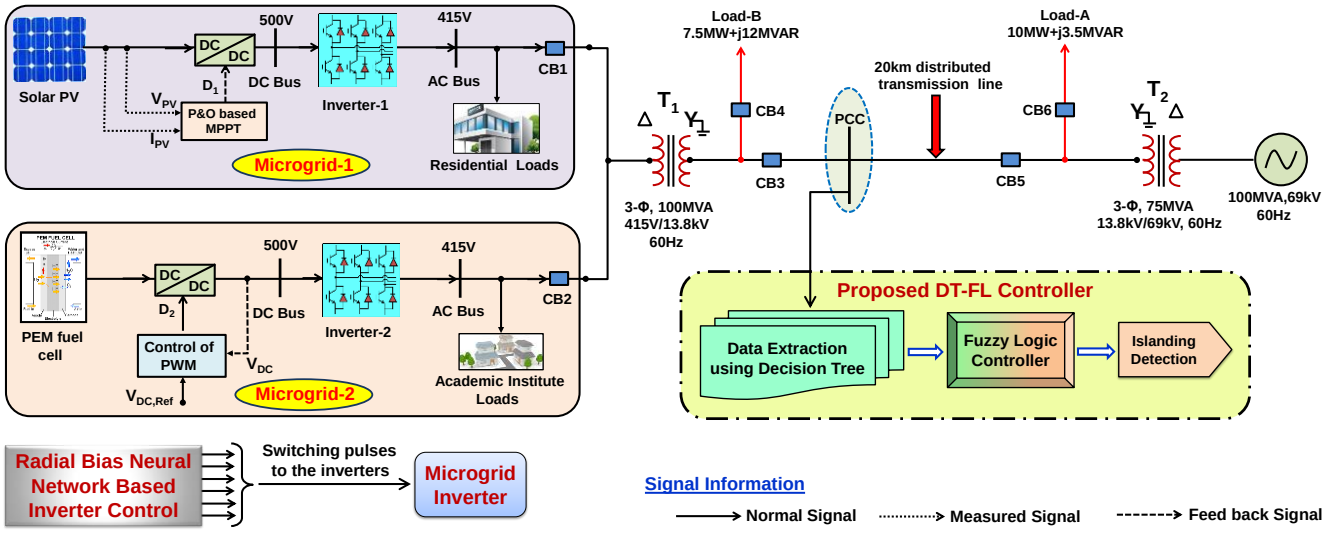

Figure 1. Schematic of urban community multi-microgrid cluster with proposed DT-FL controller.

2.1. Solar PV System Modeling

The market for photovoltaic (PV) systems is rapidly expanding in the modern world as a result of the sharp rise in the price of fossil fuels as well as efforts to reduce greenhouse gas emissions. PV models are among the several modeling techniques that are accessible. In this work, however, we have focused on one diode model of a PV system, as illustrated in Figure 2a, and the characteristics are shown in Figure 2b, demonstrating its advantages. Although two-diode models are more accurate, they take into account combination losses in the solar cell depletion zone. Moreover, two-diode and three-diode models provide many benefits because adding extra diodes to a structure increases the computational complexity. When compared to other models, the single-diode model is precise and easy to build. In this work, the perturb and observation MPPT algorithm is adopted [20]; the implementation is shown in Figure 2c. The mathematical modeling of the solar PV system can be obtained from Figure 2a and is given in Equations (1) to (4) [21].

$$\vec{I}_p = \left[\vec{I}_{sc} + \mathrm{T}_{sc}(\mathrm{T} - 298)\right] * \vec{I}_R * 10^{-3} \tag{1}$$

$$\vec{I}_{rs} = \vec{I}_{sc} * \left[\exp\left(\frac{q.V_{oc}}{n_s KAT}\right) - 1\right]^{-1} \tag{2}$$

$$\vec{I}_0 = \vec{I}_{rs}\left(\frac{\mathrm{T}}{\mathrm{T}_N}\right)^3 * \exp\left(\frac{qE_{g0}}{AK}\left(\frac{1}{\mathrm{T}_N} - \frac{1}{\mathrm{T}}\right)\right) \tag{3}$$

$$\vec{I} = N_p * \vec{I}_p - N_p * \vec{I}_0 * \exp\left(\frac{q\left(\frac{V}{N_s} + I.\frac{R_s}{N_p}\right)}{A.\left(\frac{K.\mathrm{T}_N}{q}\right)} - 1\right) - \frac{1}{R_{sh}}\left(V.\frac{N_p}{N_s} + I.R_s\right) \tag{4}$$

where $\vec{I}_p$—photocurrent, $\vec{I}_{sc}$—current under short circuit (*SC*), T_{sc}—temperature under *SC*, T—operating temperature of the cell, $\vec{I}_R$—cell irradiance current, $\vec{I}_{rs}$—reverse saturation current, q—charge, V_{oc}—open circuit voltage, K—Boltzmann's constant, A—ideal factor, N_s—series-connected cells, N_p—parallel-connected cells, $\vec{I}_0$—saturation current of the module, T_N—nominal temperature, $\vec{I}$—output current, E_{g0}—semiconductor energy gap, R_s—series resistance, V—voltage of the diode.

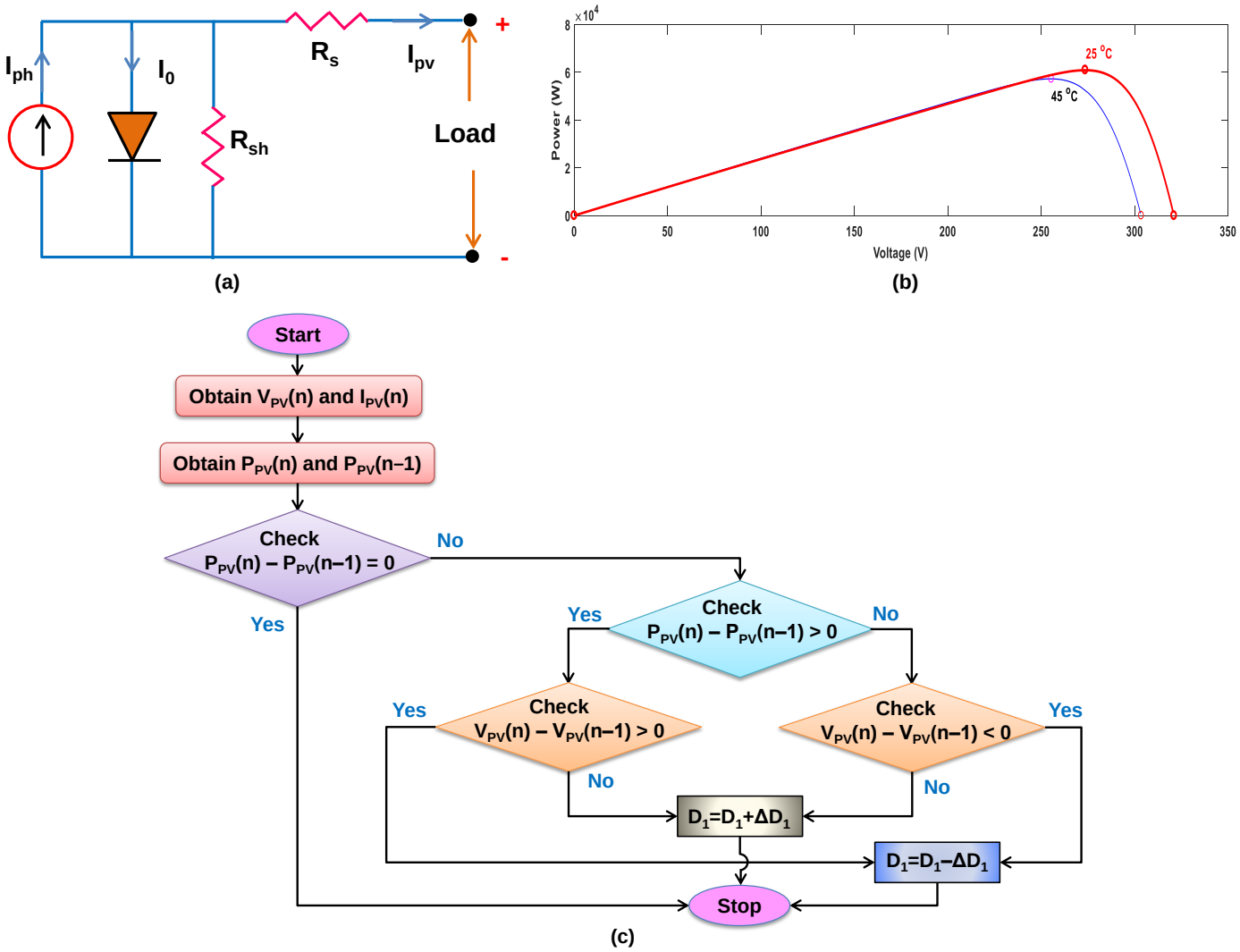

Figure 2. Solar PV system. (**a**) Equivalent circuit. (**b**) P-V characteristics. (**c**) P&O MPPT algorithm.

2.2. Proton Exchange Membrane Fuel Cell (PEMFC) Modeling

Without a battery, fuel cells are electrochemical devices that convert chemical energy into electrical energy. Because of the electrolyte used in the cell, a proton exchange membrane fuel cell was taken into consideration for this work. An electrolyte is contained in the proton exchange membrane fuel cell (PEMFC), connected between the anode and cathode chambers. In a PEM fuel cell, oxygen from the atmosphere enters the compartment of the cathode, while fuel from gases enters the anode. Thus, electrochemical processes occur to produce a current. The equation of 'Nernst' for the calculation of the thermodynamic energy 'E_n' is considered for fuel cell modeling, as given in Equations (5) to (7) [21].

$$E_n = (1.27616 - 0.00008 * \mathrm{T}) + \left(0.0000045 \times \mathrm{T} \times \left(\ln \mathrm{P}_{H_2} + \ln \mathrm{P}_{O_2}\right)\right) \quad (5)$$

$$Disolved_{oxyzen} = \mathrm{P}_{O_2} * \left(5.08 \times 10^6 \exp\left(\frac{-498}{\mathrm{T}}\right)\right)^{-1} \quad (6)$$

$$H_2O(liquid) + Electrical\ Energy = H_2 + 0.5 * O_2(gaseous) \quad (7)$$

where P—effective pressure, T—stack temperature.

2.3. DC to DC Converter Modeling

Renewable energy sources produce inconsistent voltages at their output, which is not sufficient to meet electricity needs. As a result, to improve the performance of grid-connected renewable energy systems today, it is crucial to use a DC/DC converter that generates higher outputs for lower inputs. The fundamental operation of a DC/DC boost converter is dependent on the behavior of an inductor, which prevents abrupt changes in current while permitting changes in the inductor's magnetic field energy. The equivalent circuit of the boost converter is shown in Figure 3a, and the working principle is explained using Figure 3b,c [21].

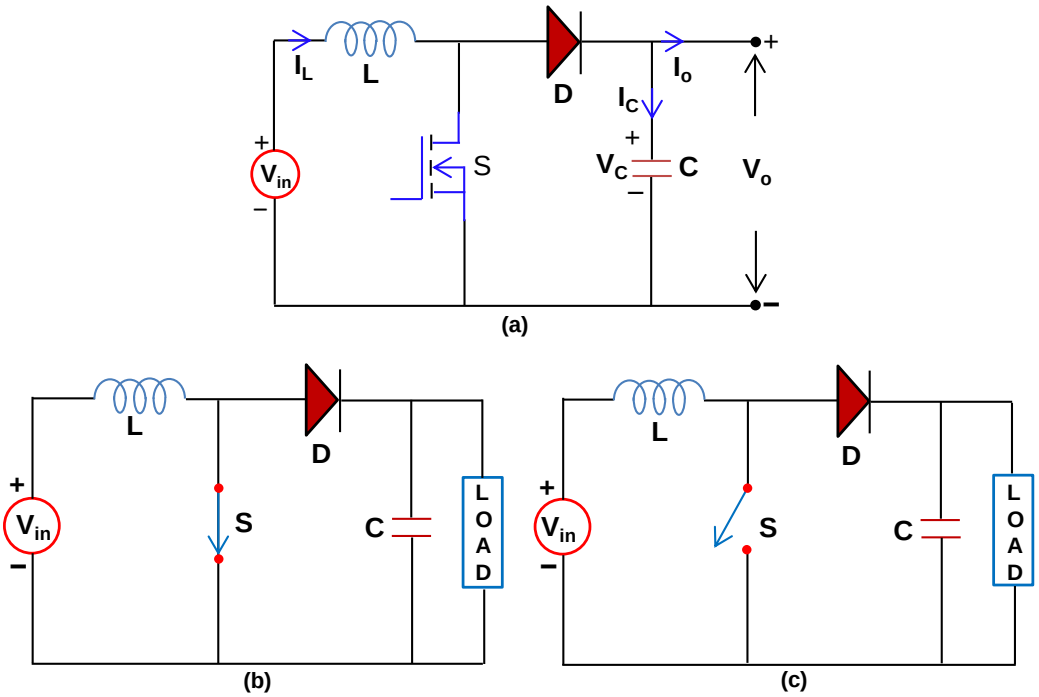

Figure 3. DC-DC converter. (**a**) Equivalent circuit, (**b**) ON state depiction, (**c**) OFF state depiction.

During the ON state, the inductor starts charging and stores magnetic energy, and, during the OFF state, the current decreases, thereby increasing the impedance of the circuit. The state space equations of the converter are given in Equations (8) to (10).

$$\frac{dI_L}{dt} = -V_C\left(\frac{1-D}{L}\right) + \frac{V_{in}}{L} \tag{8}$$

$$\frac{dV_c}{dt} = I_L\left(\frac{1-D}{C}\right) + \frac{V_c}{RC} \tag{9}$$

$$V_0 = V_C \tag{10}$$

Here, I_L—inductor current, V_C—capacitor voltage, D—duty ratio.

2.4. Control Circuit for DC to AC Converter (Three-Phase Inverter) Modeling

In general, the power electronic inverter is crucial for renewable-energy-based microgrid systems due to its effective functioning. Nowadays, artificial-intelligence-based control techniques to produce the required gate pulses to the inverter are gaining popularity. Keeping this in view, in this work, a radial basis neural network is trained for the tuning of the PI controller. The Simulink implementation of the control circuit for the production of gate pulses to the inverter is shown in Figure 4.

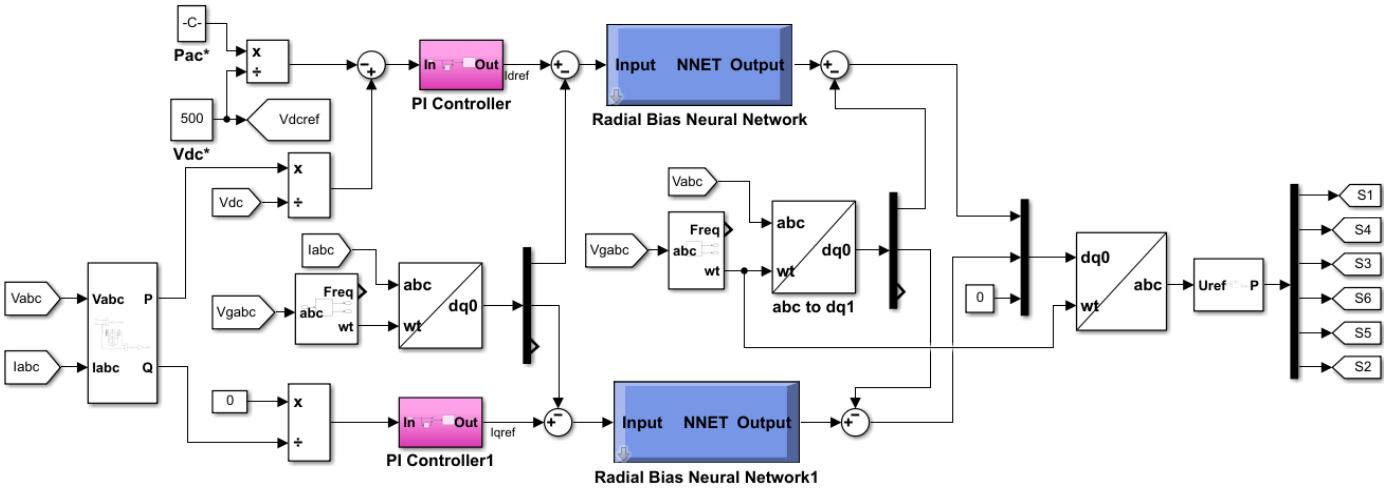

Figure 4. Control circuit for production of required gate pulses to the inverter of *i*th MG.

2.5. Load Profiles Considered for Modeling of MG-1 and MG-2

In this case study, a 20-flat residential building is considered for MG-1 modeling, and a small academic institute building is considered for MG-2 modeling. The types of loads and their distribution in a day are assumed as shown in Tables 1–3. For simulation, a 4-h duration in a day is assumed as 0.05 s.

Table 1. Loads considered for modeling of MG-1 and MG-2 based on assumptions.

S. No.	Load Name	Load Type	Rating (kW + jkVAR)
1	Fan	Load-1	0.07 + j0.019
2	Light	Load-2	0.03 + j0.006
3	AC_type1	Load-3	1.3 + j0.429
4	TV	Load-5	0.07 + j0.019
5	Refrigerator	Load-6	0.4 + j0.14
6	Grinder	Load-7	0.5 + j0.17
7	Washing machine	Load-8	0.51 + j0.16
8	Computer	Load-9	0.46 + j0.148
9	Water cooler	Load-10	0.51 + j0.16
10	Machine_type1	Load-11	2.2 + j0.724

Table 2. Assumed load profile of the residential building in MG-1.

Load Particulars			Load Distribution in a Day																	
Load Type	Qty/ Flat	Qty/ 20 Flats	0–4 h			4–8 h			8–12 h			12–16 h			16–20 h			20–24 h		
			Qty ON	Load		Qty ON	Load		Qty ON	Load		Qty ON	Load		Qty ON	Load		Qty ON	Load	
				kW	kVAR		kW	kVAR		kW	kVAR		kW	kVAR		kW	kVAR		kW	kVAR
Load-1	3	60	60	3.61	1.15	60	3.61	1.14	40	2.42	0.76	40	2.4	0.77	45	2.7	0.86	30	1.8	0.57
Load-2	4	80	20	0.4	0.12	40	0.8	0.24	25	0.5	0.15	10	0.2	0.06	60	1.2	0.36	70	1.4	0.42
Load-3	1	20	16	20.8	6.83	12	15.6	5.12	8	10.4	3.42	18	23.4	7.69	9	11.7	3.84	17	22.1	7.26
Load-5	1	20	2	0.12	0.04	12	0.72	0.23	15	0.9	0.29	15	0.9	0.29	16	0.96	0.3	15	0.9	0.29
Load-6	1	20	20	8	2.6	20	8	2.6	20	8	2.6	20	8	2.6	20	8	2.6	20	8	2.6
Load-7	1	20	2	1	0	14	7	1.12	14	7	2.24	4	2	0.64	5	2.5	0.8	10	5	1.6
Load-8	1	20	0	0	0	10	5	0.8	15	7.5	2.4	6	3	0.96	8	4	1.28	8	4	1.28
Total Load			33.9 + j10.73			40.72 + j11.25			36.7 + j11.86			39.9 + j13			31.06 + j10			47.1 + j14.02		

Table 3. Assumed load profile of the academic institute building in MG-2.

Load Details		Load Distribution over a Day																	
Load Type	Qty/Flat	0–4 h			4–8 h			8–12 h			12–16 h			16–20 h			20–24 h		
		Qty ON	Load		Qty ON	Load		Qty ON	Load		Qty ON	Load		Qty ON	Load		Qty ON	Load	
			kW	kVAR		kW	kVAR		kW	kVAR		kW	kVAR		kW	kVAR		kW	kVAR
Load-1	200	20	1.2	0.38	40	2.4	0.76	150	9	2.85	180	10.8	3.42	70	4.2	1.33	50	3	0.95
Load-2	300	50	1	0.3	25	0.5	0.15	150	3	0.9	150	3	0.9	50	1	0.3	120	2.4	0.72
Load-3	25	5	6.5	2.14	5	6.5	2.14	10	13	4.27	15	19.5	6.41	10	13	4.27	7	9.1	2.99
Load-9	150	20	9	2.96	40	18	5.92	75	33.75	11.1	100	45	14.8	80	36	11.84	50	22.5	7.4
Load-11	10	0	0	0	0	0	0	7	15.4	5.06	7	15.4	5.06	0	0	0	0	0	0
Load-10	20	10	5	1.6	10	5	1.6	20	10	3.2	20	10	3.2	10	5	1.6	10	5	1.6
Total Load		22.7 + j7.38			32.4 + j10.57			84.15 + j27.38			103.7 + j33.79			59.2 + j19.34			22 + j13.66		

3. Proposed Decision-Tree-Based Fuzzy Logic (DT-FL) Controller

The proposed decision-tree-based fuzzy logic controller adopts a passive method by taking the data mining methodology into account for islanding detection in a multi-microgrid cluster. This process involves creating a straightforward and reliable fuzzy classifier with an initial decision tree for islanding detection. It becomes vital to address structural problems with the identification of classifier systems as a result of the complexity and dimensionality of the classification problems arising. The identification of the appropriate initial partition of the input domain and the choice of pertinent features are important considerations. Moreover, when the classifier is recognized as a component of an expert system, language interpretability is another crucial factor that needs to be taken into consideration. While the interpretability factor is frequently unnoticed, the first two aspects are frequently tackled through educated estimates. When the significance of each of these factors is understood, automatic data-based classification systems that are accurate, compact, and understandable may be identified.

The input space is divided into rectangles by DT-based classifiers, whereas fuzzy models produce non-axis parallel decision boundaries. Because of this, rule-based classifiers have more flexible decision bounds than crisp DTs, which is their main advantage. As a result, fuzzy classifiers may be easier to understand than DT classifiers. The suggested method is implemented mainly in two stages: (1) features are extracted in the first stage, and (2) a classification task is carried out in the second stage to detect islands. Hence, one of the crucial responsibilities associated with the suggested approach is feature selection. Thus, we have obtained the change in frequency deviation, change in voltage deviation, and rate of change in frequency at the point of common coupling of the MMG. The decision tree uses the extracted features as inputs to select the most important aspects that contribute to the decision-making process and the initial categorization limits. Trapezoidal fuzzy membership functions are generated from the DT classification boundaries of the most significant features, and a corresponding rule base is formed for classification. However, depending on the similarity measure, certain fuzzy MFs are combined, which lowers the overall number of fuzzy MFs. A streamlined fuzzy rule basis for islanding detection is created from the fuzzy MFs that have been decreased in size. A DT is a high-dimensional classifier DT, in which each branch of the tree indicates the result of a test, while each internal node evaluates the usefulness of a predictor. The leaf nodes, also known as the ending nodes, reflect the classification. The classification problem's dimension is indicated by how many predictors are utilized. The confidence in the decision is connected to each decision (tree leaf). In simple terms, this is the ratio of the specific class to all the other classes in the dataset for a given node [22].

A robust, accessible data mining and analysis workbench called "Insightful Miner" enables enterprises to provide tailored predictive intelligence whenever required. Its user-friendly interface was created with statisticians and business analysts, who lack specialist programming skills, in mind. With Insightful Miner, one can identify the solutions that

one needs to tackle particular business problems quickly and effortlessly and share one's findings with one's colleagues throughout the company. Insightful Miner performs better in this scenario by offering a strong statistical analysis and visualization capacity, as typical data mining tools become less and less effective as the data sets grow in size. Hence, for the suggested study, this has been chosen to develop the DT structure. The most relevant characteristics that are used in the decision-making process are produced by the DT analysis using the best splitting setting, which includes the extracted features at the PCC. In this study, a total of 11 features are extracted at the PCC of the multi-microgrid system, which are given in Table 4. However, in the end, the classification tree shown in Figure 5 is developed using only three features. As a result, DT only gives information on the three most important features that influence the decision making, rendering the remaining eight features superfluous. Fuzzy membership functions are created from the categorization boundaries of the most significant characteristics produced by DT and used in the fuzzy rule basis for islanding.

Table 4. Extracted features at PCC of the system.

Extracted Feature at PCC	Notation	Units
Change in frequency	Δf	Hz
Change in voltage	ΔV	PU
Rate of change in frequency	$\frac{d}{dt}(\Delta f)$	Hz/s
Rate of change in voltage	$\frac{d}{dt}(\Delta V)$	PU/s
Rate of change in power	$\frac{d}{dt}(\Delta P)$	MW/s
Ratio of change in frequency to change in power	$\frac{\Delta f}{\Delta P}$	Hz/MW
Current THD	I_{THD}	PU
Voltage THD	V_{THD}	PU
Change in power factor	ΔPF	--
Absolute phase voltage times of power factor	$U\cos\theta$	--
Rate of change of absolute phase voltage times of power factor	$\frac{d}{dt}U\cos\theta$	--

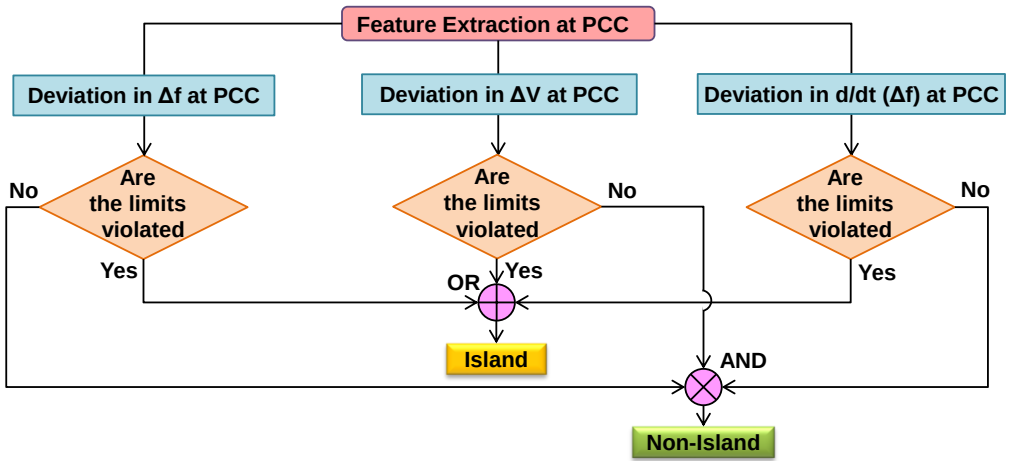

Figure 5. Structure of decision-tree-based classifier for detection of islands.

After obtaining the DT's partition boundaries from the classification, we create fuzzy membership functions and the DT is converted into a fuzzy rule base. Rectangular MFs are created for each independent variable from the DT boundaries. The process of fuzzification replaces a numerical attribute X_k with a fuzzy attribute A_k (k = 1, 2, 3 ... i) described by B_k linguistic terms. We refer to these linguistic concepts as fuzzy sets. As the numerical attribute values are defined as a vector of real numeric values, we have 'M' instances of these values $(x_1, x_2, x_3 \ldots x_M)$. Each lth numerical value of this vector $(l = 1, 2 \ldots M)$ is fuzzified into membership degrees of B_k linguistic terms. As a result, these values of the membership function of each B_k linguistic concept define the value of each instance of the fuzzy attribute.

Thus, the jth linguistic term of A_k is designated as $A_{j,k}(j = 1, 2 \ldots B_k)$. Fuzzy set $A_{j,k}$ with respect to X_k is defined by a membership function $\mu A_{j,k}(x) : X_k \rightarrow (0, 1)$. Formally, a fuzzy set $A_{j,k}$ is described in terms of a pair of sets given by $A_{j,k} = \left[\left(x, \mu A_{j,k}(x)\right), x \in X_k\right]$ [23]. The DT output obtained from the aforementioned DT-fuzzy transformation method is changed into the corresponding fuzzy rule base. Three input parameters extracted from the PCC of the MMG cluster are designated as 'X_1', which is a change in frequency deviation, 'X_2', which is a change in voltage deviation, and 'X_3', which is the rate of change in the frequency deviation. For islanding detection, the categorization borders are determined based on the values of the above three variables, as mentioned in Appendix A. The contour plot of the input parameters extracted at the PCC of the system considered for testing and the output parameter is shown in Figure 6.

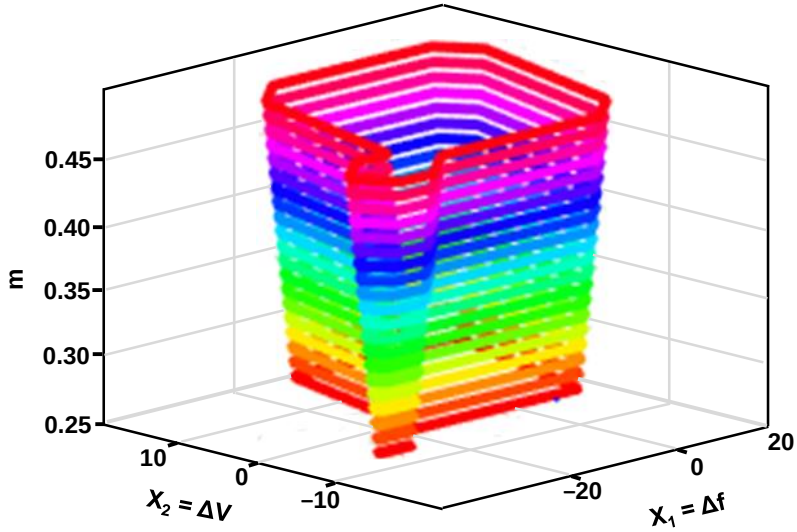

Figure 6. Contour plot of the input and output parameters.

The developed membership functions for X_1 are (P_1, P_2), for X_2 are (Q_1, Q_2, Q_3), and for X_3 are (R_1, R_2). Rectangular shapes characterize the fuzzy MFs produced by the DT classification boundaries. However, the rectangular borders are somewhat warped by heuristic adjustment, which adds fuzziness to the membership functions. Following tests on numerous values in the vicinity of the starting values produced from the DT, the coordinates of the trapezoidal fuzzy MFs are adopted. The fuzzy membership function plots of the input and output variables are shown in Figure 7. The flow chart implementation for the proposed DT-based fuzzy logic controller is shown in Figure 8.

The corresponding fuzzy rules are formed as follows.

- Rule 1: if X_1 is P_1 and X_2 is Q_2, then an island occurs.
- Rule 2: if X_1 is P_2 and X_2 is Q_3, then an island occurs.
- Rule 3: if X_1 is P_2 and X_2 is Q_1 and X_3 is R_1, then an island occurs.
- Rule 4: if X_1 is P_2 and X_2 is Q_1 and X_3 is R_2, then no island occurs.

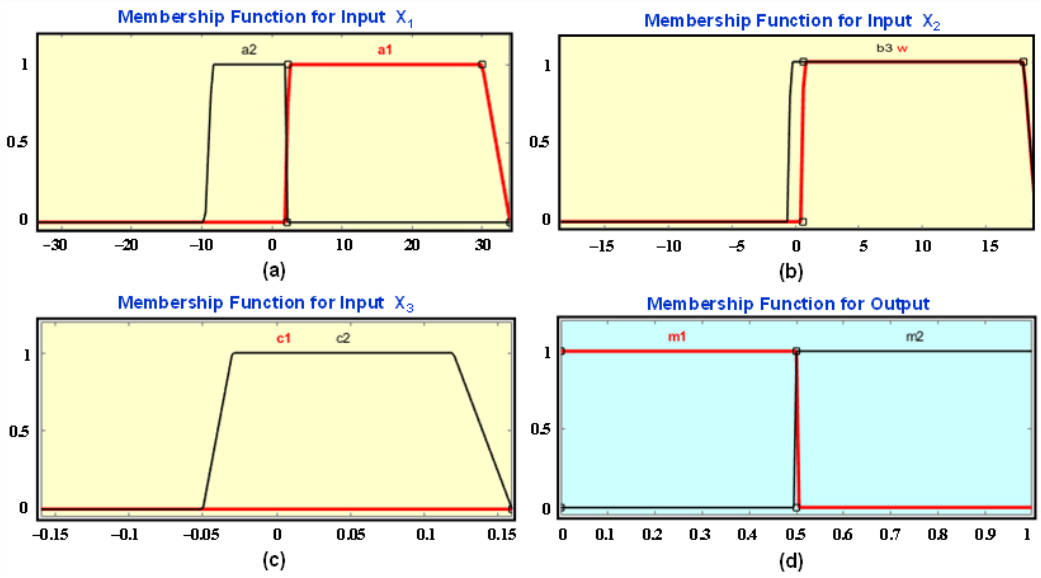

Figure 7. Membership function plots of input and output variables. (**a**) for input X_1, (**b**) for input X_2, (**c**) For input X_3, (**d**) for output.

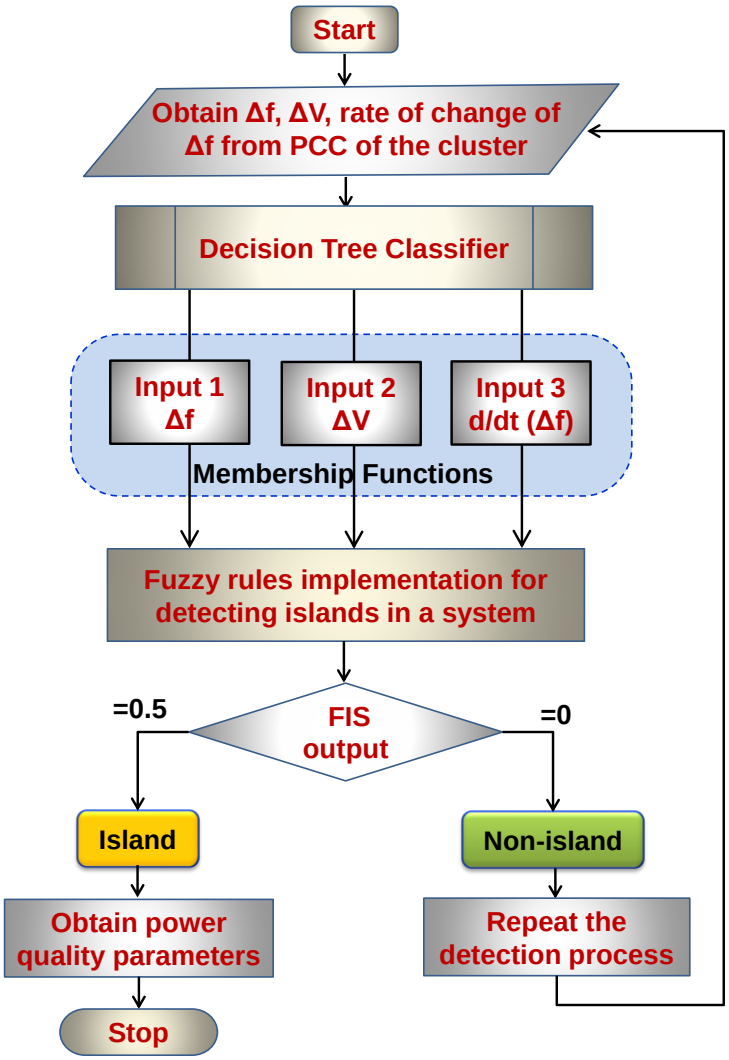

Figure 8. Flow chart implementation for the proposed DT-FL controller.

4. Simulation Results and Discussion

To identify the performance of the proposed DT-FL controller for the detection of an island in a multi-microgrid cluster, different test conditions are considered. The obtained characteristics are then compared with the conventional fuzzy controller to understand the effectiveness of the proposed methodology. The system under study, along with the DT-FL, is modeled in the MATLAB software 2021a, ver. 9.1, for a 64-bit PC. The test conditions considered for the identification of islanding in a system with the proposed DT-FL controller are shown in Table 5.

Table 5. Various testing scenarios considered for the simulation.

S. No.	Condition	Description of Procedure
1	A	Trip the circuit breaker (CB_1) of MG-1 by connecting a PCC load of 7.5 MW + j12.5MVAR
2	B	A sudden drop in the loads connected at the PCC by 25%, i.e., 1.89 MW + j3MVAR
3	C	Trip the circuit breaker (CB_2) of MG-2 by isolating the PCC loads

4.1. Analysis of the System under Test Condition A

When 'condition A', which is given in Table 5, is executed, the input values extracted using the DT are $\Delta f = 3.19$; $\Delta V = 1.05$; and $\frac{d(\Delta f)}{dt} = 0.16$. However, as per the fuzzy rule base developed from Equations (11) to (14), the FIS output generated by the system corresponding to these input parameters is '0.5', which the condition defines as an "island", as shown in Figure 8. Further, the input and output parameters that are obtained during online extraction are shown in Figure 9.

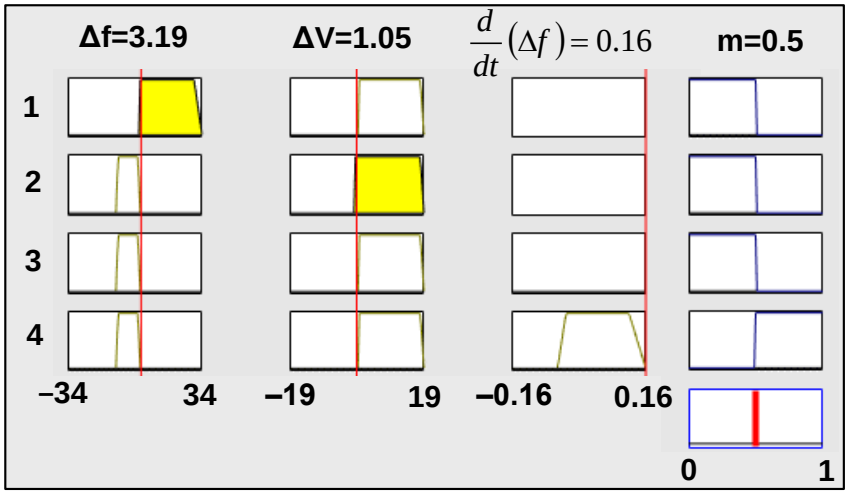

Figure 9. FIS output produced with extracted parameters.

Later, the analysis is further extended to study the frequency response, voltage characteristics at the PCC of the multi-microgrid system, and total harmonic distortion (THD) during the execution of test condition A. From the frequency response shown in Figure 10, it is observed that the islanding condition is quickly identified by the proposed DT-FL and conventional FL controllers at 0.02 s. This is satisfactory according to IEEE Std. 1547-2003 [24,25]. At 0.02 s, the deviation in the frequency with the conventional FL controller is higher and it is greater than ±5% when compared with the proposed DT-FL controller. From the voltage characteristics shown in Figure 11, it is observed that the settling time of the system with the conventional FL controller after the occurrence of the islanding condition is greater compared to the proposed DT-FL controller. Because of the large settling time, the transient response is poor with the conventional FLC, whereas the transient response of the system is improved with the proposed DT-FL controller.

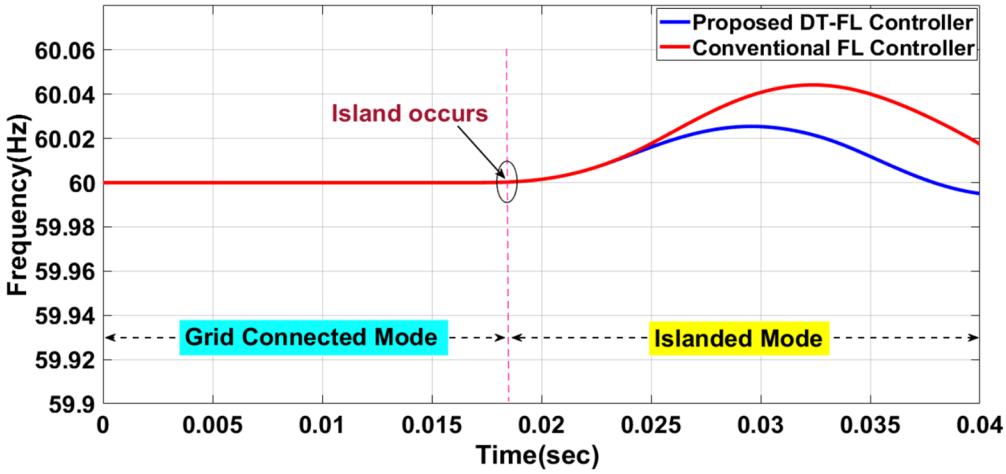

Figure 10. Frequency at PCC of the system with conventional FL and proposed DT-FL controllers.

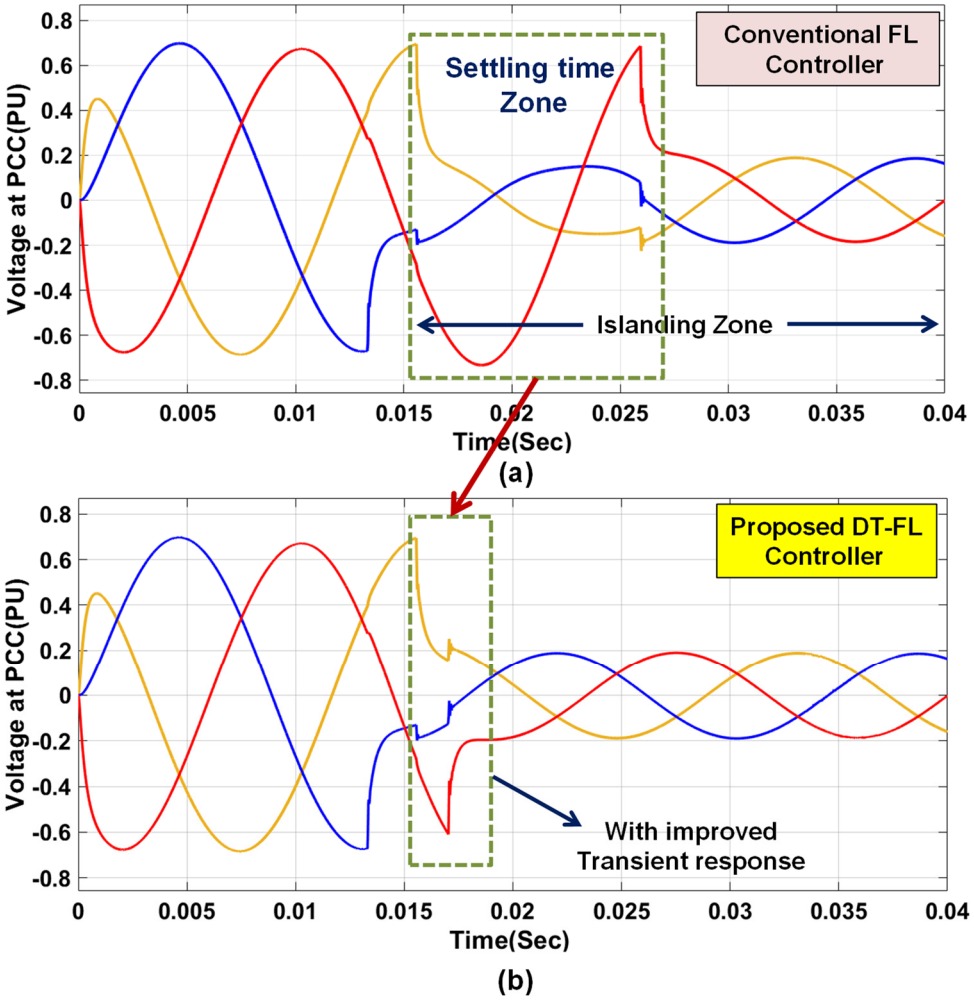

Figure 11. Voltage profile at PCC with (**a**) conventional FL control and (**b**) proposed DT-FL controller.

The THD plot of the system is shown in Figure 12. From the plot, it is observed that with the conventional FL controller, the THD is 7.05%, and with the proposed DT-FL controller, the THD is 4.10%. Thus, from this discussion, it is observed that with test condition A, the proposed DT-FL controller gives good results.

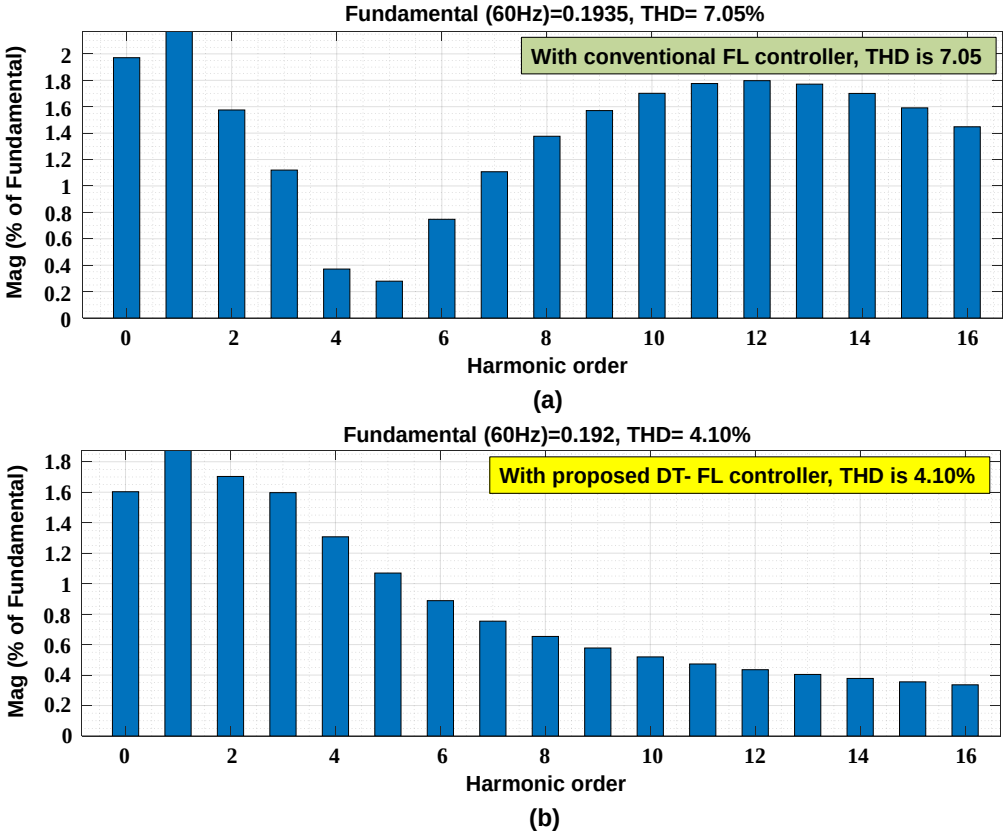

Figure 12. THD of the system with (**a**) conventional FL and (**b**) proposed DT-FL controller.

4.2. Analysis of the System under Test Condition B

When 'condition B', shown in Table 5, is executed, $\Delta f = 3.087$, $\Delta V = 0.95$, and $\frac{d}{dt}(\Delta f) = 0.16$ are the input values extracted using DT. With the fuzzy rule base developed from Equations (11) to (14), the FIS output produced by the system corresponding to these input parameters is '0.5', which is also the condition for the island. The input and output parameters obtained during online extraction are shown in Figure 13. The analysis of the system is carried out from the frequency response, voltage plot, and THD plot.

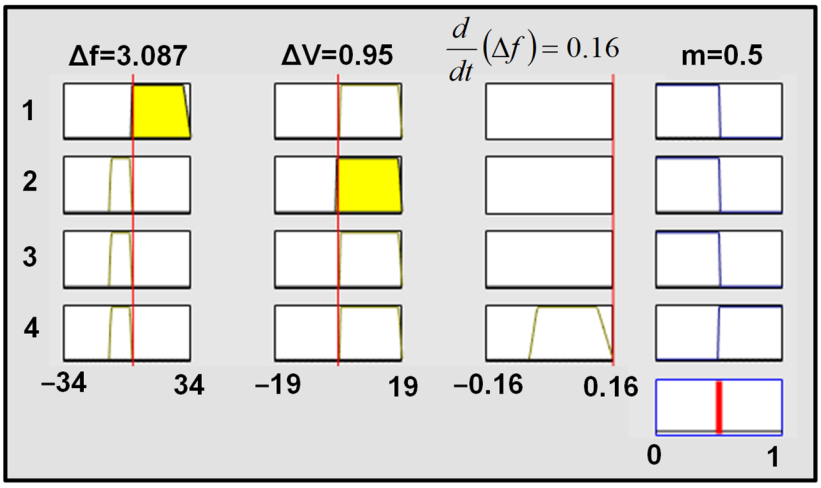

Figure 13. FIS output produced with extracted parameters.

From Figure 14, it is observed that after 0.02 s, i.e., immediately after the occurrence of the island, the deviation in the frequency with the conventional FL is larger than that with

the proposed DT-FL controller, which may lead to the system's instability. This situation can be minimized with the proposed DT-FL controller.

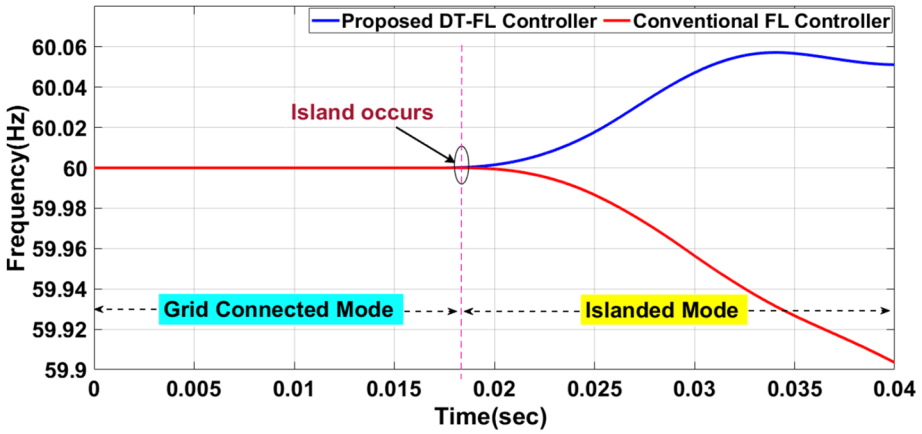

Figure 14. Frequency at PCC of the system with conventional FL and proposed DT-FL controllers.

From the voltage characteristics shown in Figure 15, it is observed that a more distorted waveform is obtained with the conventional FL controller when a sudden load dismissal occurs at the PCC, whereas a smooth voltage waveform is obtained with the proposed DT-FL controller despite the load removal. From the THD plot of the system, shown in Figure 16, it is observed that with the conventional FL controller, the THD is 15.01%, and with the proposed DT-FL controller, the THD is improved and is 5.35%. However, in both cases, the THD is not within the limits defined by the IEEE standards. Nonetheless, during this test condition, the proposed DT-FL controller performed better than the conventional FL controller.

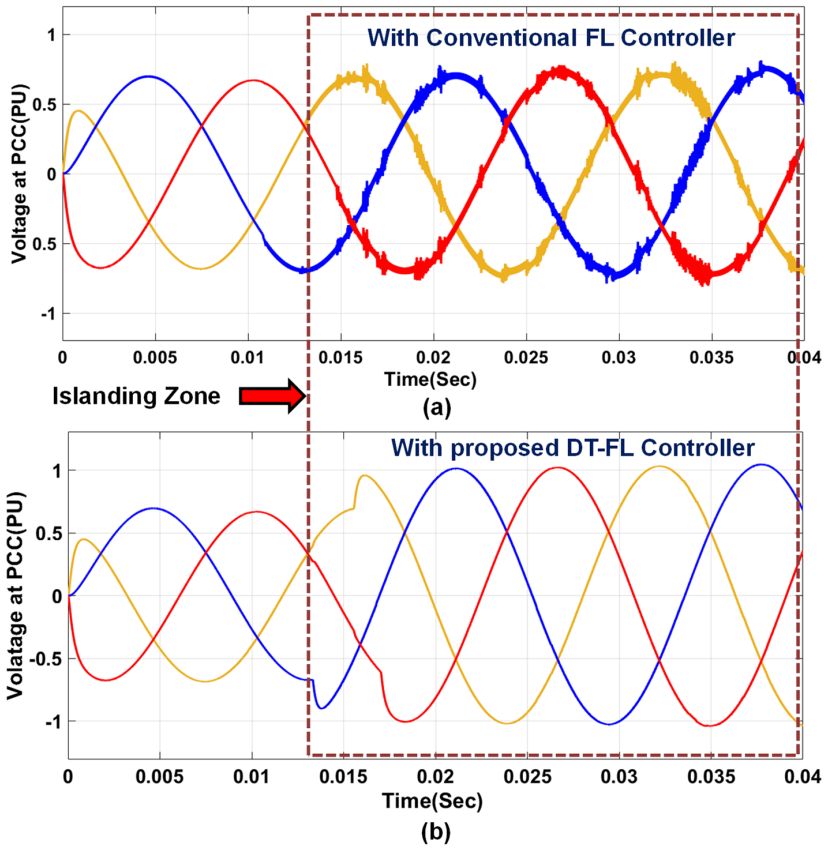

Figure 15. Voltage profile at PCC with (**a**) conventional FL and (**b**) proposed DT-FL controller.

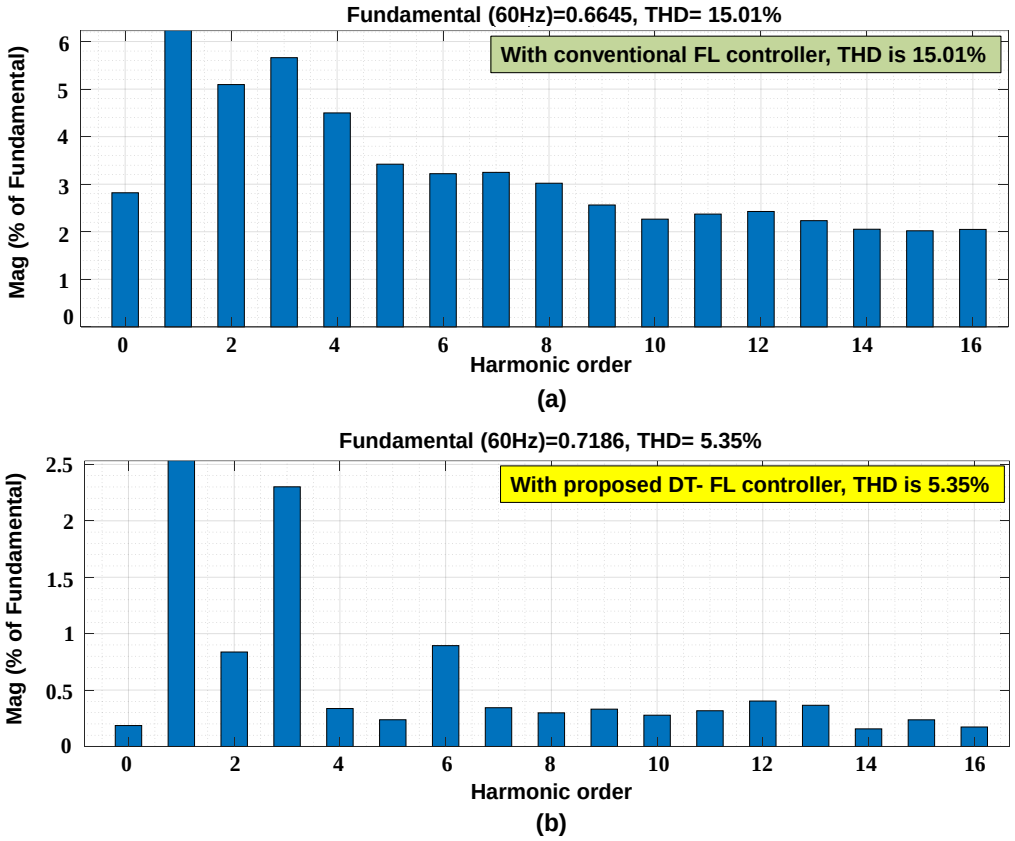

Figure 16. THD of the system with (**a**) conventional FL and (**b**) proposed DT-FL controller.

4.3. Analysis of the System under Test Condition C

When 'condition C', shown in Table 5, is executed, the input parameters extracted using DT are also the same as in test condition 1, shown in Figure 9. In this case, the tripping of CB_2 for MG-2 causes the generation of the FIS output corresponding to these input parameters to be '0.5'. During the analysis, it is identified that the same frequency response is obtained with both the conventional FL and proposed DT-FL controllers, which is shown in Figure 17. However, there is a voltage drop with the conventional FL controller. This voltage is increased with the use of the proposed DT-FL controller, as shown in Figure 18.

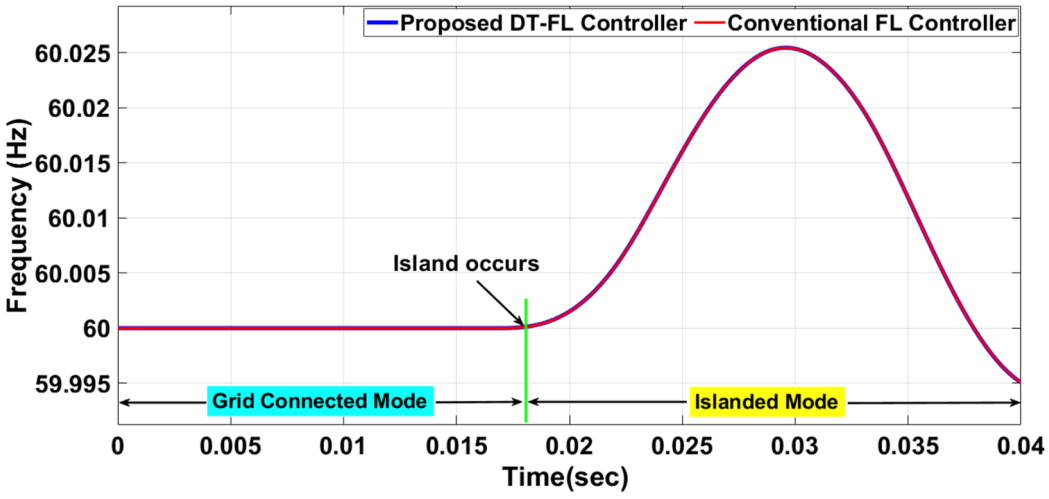

Figure 17. Frequency at PCC of the system with conventional FL and proposed DT-FL controllers.

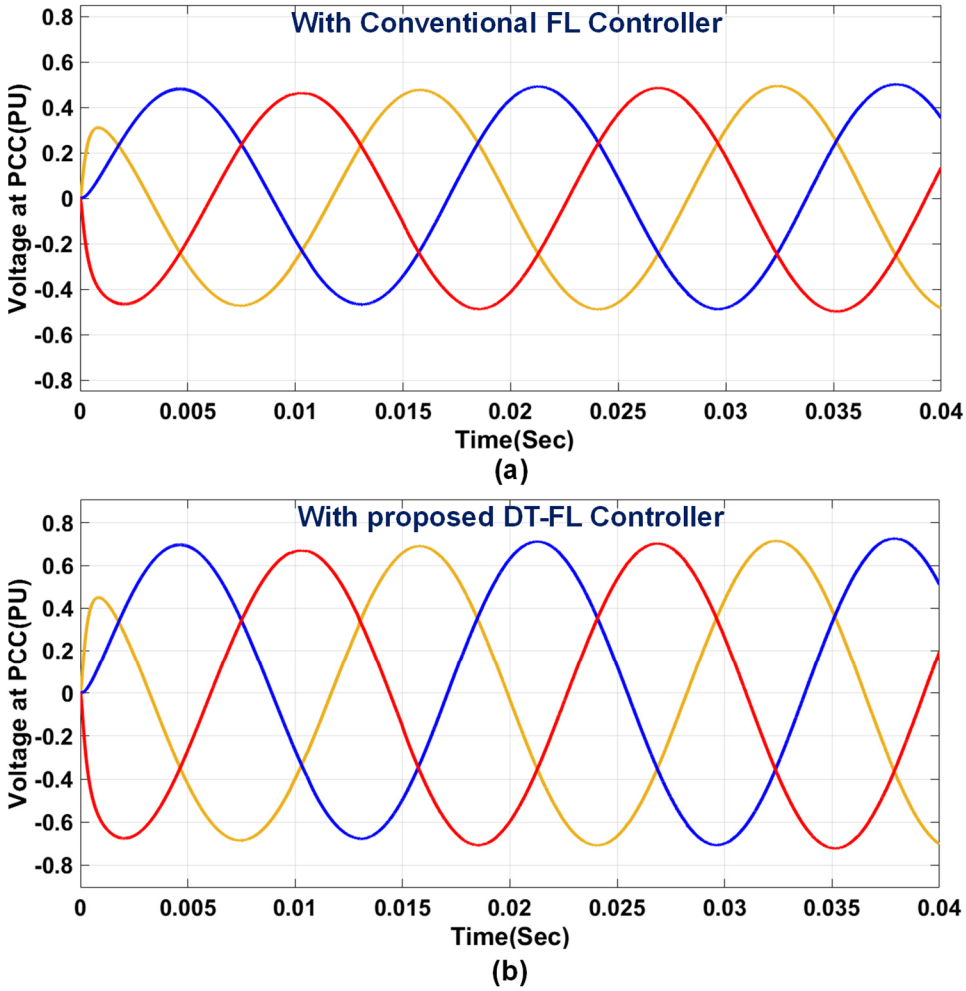

Figure 18. Voltage profile at PCC with (**a**) conventional FL and (**b**) proposed DT-FL controller.

From the THD plot of the system, shown in Figure 19, it is observed that the THD value with the conventional FL controller is computed as 2.50%, while it is improved and computed as 1.03% with the proposed DT-FL controller. In both cases, the THD is within the limits defined by the IEEE standards. Thus, during all the test conditions given in Table 6, the proposed DT-FL controller performs better than the conventional FL controller with respect to power quality indices such as the frequency response, voltage fluctuations, and the THD of the system.

Similarly, Table 6 shows the performance comparison between the conventional and proposed DT-based fuzzy logic controllers. In this work, a total of 10 test cases were considered to verify the accuracy of the conventional and proposed controllers with and without noise. From Table 6, quantitatively, it is observed that the proposed DT-FL controller effectively gives better results.

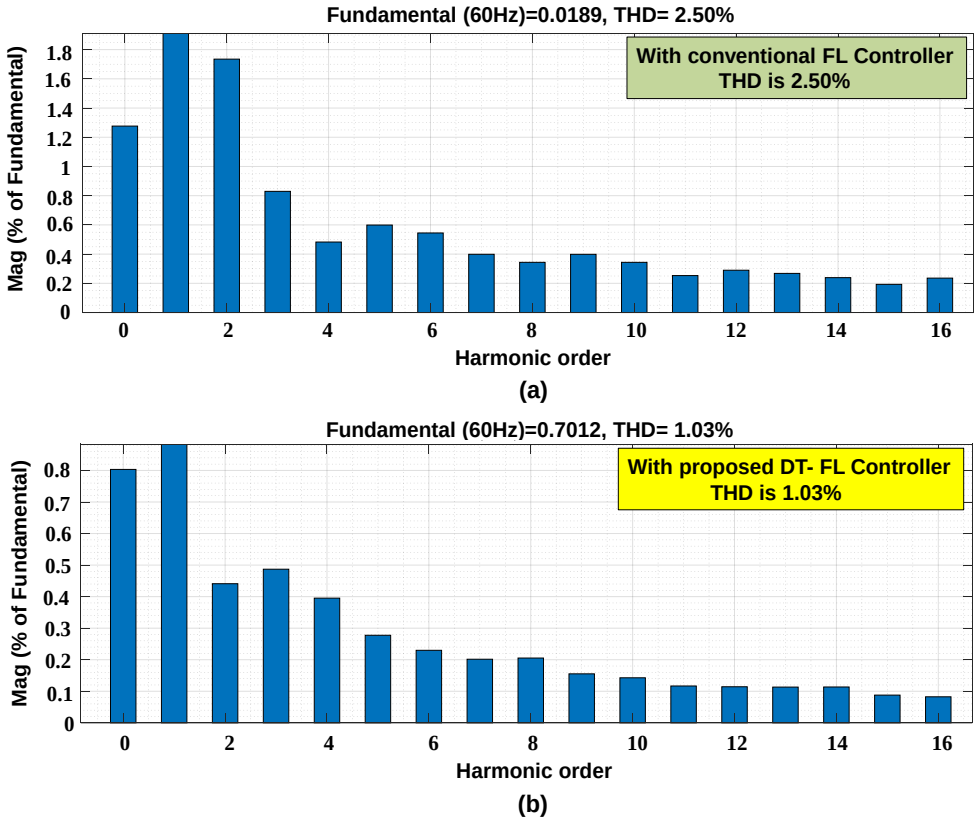

Figure 19. THD of the system with (**a**) conventional FL and and (**b**) proposed DT-FL controller.

Table 6. Performance comparison of conventional and proposed DT-FL controllers.

Test Cases	Actual Class	Conventional FL Controller without Noise		
		FIS-0.5 (Island)	**FIS-0 (Non-Island)**	**Accuracy (%)**
10	Island	8	0	80
	Non-island	0	8	80
		Proposed DT-FL Controller without Noise		
		FIS-0.5 (Island)	**FIS-0 (Non-Island)**	**Accuracy (%)**
	Island	10	0	100
	Non-island	0	10	100
		Conventional FL Controller with Noise (20 dB)		
		FIS-0.5 (Island)	**FIS-0 (Non-Island)**	**Accuracy (%)**
	Island	7	0	70
	Non-island	0	7	70
		Proposed DT-FL Controller with Noise (20 dB)		
		FIS-0.5 (Island)	**FIS-0 (Non-Island)**	**Accuracy (%)**
	Island	9	0	90
	Non-island	0	9	90

5. Conclusions

In this paper, a DT-based FL controller for fast islanding detection in an urban community multi-microgrid cluster is proposed. The decision tree is used to extract the features through the PCC of the system under study. The proposed DT-FL controller's performance is compared with that of the conventional FL controller, which proves its superiority. A summary of the achievements is given as follows.

- Islanding detection is achieved satisfactorily, with better transient response characteristics for the voltage and frequency.
- The THD limits are also maintained as per the IEEE standards.
- The frequency response is maintained within the limits suggested by the IEEE standards, using the proposed DT-FL controller.
- The transient response of the system is improved by reducing the settling time after the occurrence of the island.

Thus, the proposed DT-FL controller helps to achieve smooth and rapid islanding detection and an improved transient response in grid-connected urban community multi-microgrid clusters.

Author Contributions: Conceptualization, Y.V.P.K.; Data curation, S.N.V.B.R.; Formal analysis, Y.V.P.K.; Funding acquisition, Y.V.P.K.; Investigation, S.N.V.B.R.; Methodology, S.N.V.B.R.; Project administration, R.K.; Resources, R.K.; Software, Y.V.P.K.; Supervision, R.K.; Validation, S.N.V.B.R.; Visualization, R.K.; Writing—original draft, Y.V.P.K.; Writing—review and editing, Y.V.P.K. and S.N.V.B.R. All authors have read and agreed to the published version of the manuscript.

Funding: This research was funded by the SERB International Research Experience (SIRE) scheme of the Science and Engineering Research Board (SERB), a statutory body under the Department of Science and Technology (DST), Government of India, with grant number SIR/2022/000760.

Data Availability Statement: Not applicable.

Conflicts of Interest: The authors declare no conflict of interest.

Appendix A

Table A1. The ratings of the components considered for modeling in Simulink.

Parameter	Typical Ratings
AC voltage of MG-1 and MG-2	415 V
DC voltage of MG-1 and MG-2	500 V
Transformer T_1	415 (Δ)/13.8 kV (Y-Gnd), 60 Hz
Transformer T_2	13.8 kV (Y-Gnd)/69 kV (Δ), 60 Hz
Length of distributed transmission line	20 kM
Load A	10 MW + j3.5MVAR
Load B	7.5 MW + j12MVAR
Solar PV open circuit voltage	50 V
Solar PV short circuit current	4.5 A
Fuel cell stack temperature	343 K
Fuel cell no-load voltage	0.75 V
Frequency limits	59.95 Hz–60.05 Hz
Voltage limits	0.8 PU to 1.2 PU
THD limits	5%
M.F. P_1	[2.18, 2.3, 30, 34]
M.F. P_2	[−9.5, −8.5, 1.95, 2.18]
M.F. Q_1	[0.64, 0.6, 18, 19]
M.F. Q_2	[−0.5, −0.4, 18, 19]
M.F. Q_3	[−0.5, −0.4, 0.55, 0.64]
M.F. R_1	[0.16, 0.2, 0.5, 0.6]
M.F. R_2	[−0.05, −0.03, 0.12, 0.16]
FIS output: Islanding	0.5
FIS output: Non-Islanding	0
Utility grid power	100 MVA
Utility grid voltage	69 kV
Frequency	60 Hz

References

1. Rao, S.N.V.B.; Yellapragada, V.P.K.; Padma, K.; Pradeep, D.J.; Reddy, C.P.; Amir, M.; Refaat, S.S. Day-Ahead Load Demand Forecasting in Urban Community Cluster Microgrids Using Machine Learning Methods. *Energies* **2022**, *15*, 6124. [CrossRef]
2. Reddy, G.P.; Kumar, Y.V.P.; Chakravarthi, M.K. Communication Technologies for Interoperable Smart Microgrids in Urban Energy Community: A Broad Review of the State of the Art, Challenges, and Research Perspectives. *Sensors* **2022**, *22*, 5881. [CrossRef] [PubMed]
3. Pavan Kumar, Y.V.; Bhimasingu, R. Review and retrofitted architectures to form reliable smart microgrid networks for urban buildings. *IET Netw.* **2015**, *4*, 338–349. [CrossRef]
4. Pavan Kumar, Y.V.; Bhimasingu, R. Optimal Sizing of Microgrid for an Urban Community Building in South India using HOMER. In Proceedings of the IEEE International Conference on Power Electronics, Drives and Energy Systems (PEDES), Mumbai, India, 16–19 December 2014; pp. 1–6. [CrossRef]
5. Pavan Kumar, Y.V.; Ravikumar, B. Integrating Renewable Energy Sources to an Urban Building in India: Challenges, Opportunities, and Techno-Economic Feasibility Simulation. *Technol. Econ. Smart Grids Sustain. Energy* **2016**, *1*, 1. [CrossRef]
6. Rao, S.N.V.B.; Pavan Kumar, Y.P.; Amir, M.; Ahmad, F. An Adaptive Neuro-Fuzzy Control Strategy for Improved Power Quality in Multi-Microgrid Clusters. *IEEE Access* **2022**, *10*, 128007–128021. [CrossRef]
7. Rao, S.N.V.B.; Narayana, N.R.; Prasanna, T.D.; Rao, M.S.N.L.N.; Chand, P.G. Fault Detection in Cluster Microgrids of Urban Community using Multi-Resolution Technique based Wavelet Transforms. *Int. J. Renew. Energy Res.* **2022**, *12*, 1204–1215. [CrossRef]
8. *IEEE 1547*; IEEE Standard for Interconnecting Distributed Resources with Electric Power Systems. IEEE Standard: New York, NY, USA, 2003; pp. 1547–2003.
9. Pouryekta, A.; Murthy, V.K.R.; Mithulananthan, N.; Arulampalam, A. Islanding Detection and Enhancement of Microgrid Performance. *IEEE Syst. J.* **2018**, *12*, 3131–3141. [CrossRef]
10. Mlakic, D.; Baghaee, H.R.; Nikolovski, S. A Novel ANFIS-Based Islanding Detection for Inverter-Interfaced Microgrids. *IEEE Trans. Smart Grid* **2019**, *10*, 4411–4424. [CrossRef]
11. Murugesan, S.; Murali, V. Hybrid Analyzing Technique Based Active Islanding Detection for Multiple DGs. *IEEE Trans. Ind. Inform.* **2019**, *15*, 1311–1320. [CrossRef]
12. Abde, A.A.; Salem, A.A.; Oda, E.S.; Eldesouky, A.A. Islanding Detection of Microgrid Incorporating Inverter Based DGs Using Long Short-Term Memory Network. *IEEE Access* **2020**, *8*, 106471–106486. [CrossRef]
13. Kumar, P.; Kumar, V.; Pratap, R. Rate of Change of Frequency Deviation Based Unintentional Islanding Detection for Microgrids. In Proceedings of the International Conference on Control, Power, Communication and Computing Technologies (ICCPCCT), Kannur, India, 23–24 March 2018; pp. 90–95. [CrossRef]
14. Ahmed, Y.E.; Dalal Hussien, H.; Abd-Elhaleem, S.; Abozalam, B.A.; Asham, A.D. Fast and accurate islanding detection technique for microgrid connected to photovoltaic system. *J. Radiat. Res. Appl. Sci.* **2021**, *14*, 210–221. [CrossRef]
15. Ran, C.; Li, Z.; Xiong, C.; Hanping, X.; Zhang, Z.; Xuhui, H.; Qingguo, D.; Can, W. Islanding detection method for microgrids based on CatBoost. *Front. Energy Res.* **2023**, *10*, 1016754. [CrossRef]
16. Kumar, P.; Kumar, V.; Tyagi, B. Islanding detection for reconfigurable microgrid with RES. *IET Gener. Transm. Distrib.* **2021**, *15*, 1187–1202. [CrossRef]
17. Dixit, V.; Jadhwani, M.; Pandey, A.; Kazi, F. A Hybrid Islanding Detection Scheme for Grid-Tied PV Microgrid. In Proceedings of the IEEE 18th India Council International Conference, Guwahati, India, 19–21 December 2021; pp. 1–6. [CrossRef]
18. Yasser, A.E.; Amin, D.A.; Belgacem, B.; Abdelmoty, A.; Dalal, H.H.; Belal, A.A.; Abd-Elhaleem, S. An innovative hybrid method for islanding detection using fuzzy classifier for different circumstances including NDZ. *J. Radiat. Res. Appl. Sci.* **2022**, *15*, 129–142. [CrossRef]
19. Soham, D.; Sachin, O.; Pradip Kumar, S. A secured, reliable and accurate unplanned island detection method in a renewable energy based microgrid. *Eng. Sci. Technol. Int. J.* **2021**, *24*, 1102–1115. [CrossRef]
20. Salman, S.; Ai, X.; Wu, Z. Design of a P-&-O algorithm based MPPT charge controller for a stand-alone 200W PV system. *Prot. Control. Mod. Power Syst.* **2018**, *3*, 25. [CrossRef]
21. Rao, S.N.V.B.; Padma, K. ANN based Day-Ahead Load Demand Forecasting for Energy Transactions at Urban Community Level with Interoperable Green Microgrid Cluster. *Int. J. Renew. Energy Res.* **2021**, *11*, 147–157.
22. Shaik, M.; Shaik, A.G.; Yadav, S.K. Hilbert–Huang transform and decision tree based islanding and fault recognition in renewable energy penetrated distribution system. *Sustain. Energy Grids Netw.* **2022**, *30*, 100606. [CrossRef]
23. Rabcan, J.; Zaitseva, E.; Levashenko, V.; Kvassay, M.; Surda, P.; Macekova, D. Fuzzy Decision Tree Based Method in Decision-Making of COVID-19 Patients' Treatment. *Mathematics* **2021**, *9*, 3282. [CrossRef]

24. Chakravorti, T.; Patnaik, R.K.; Dash, P.K. Detection and classification of islanding and power quality disturbances in microgrid using hybrid signal processing and data mining techniques. *IET Signal Process.* **2018**, *12*, 82–94. [CrossRef]
25. Rao, S.N.V.B.; Kumar, Y.V.P.; Pradeep, D.J.; Reddy, C.P.; Flah, A.; Kraiem, H.; Al-Asad, J.F. Power Quality Improvement in Renewable-Energy-Based Microgrid Clusters Using Fuzzy Space Vector PWM Controlled Inverter. *Sustainability* **2022**, *14*, 4663. [CrossRef]